

The kinetic temperature of a molecular cloud at redshift 0.7: Ammonia in the gravitational lens B0218+357 ^{*}

C. Henkel¹, N. Jethava¹, A. Kraus¹, K.M. Menten¹, C.L. Carilli², M. Grashoff³, D. Lubowich⁴, and M.J. Reid⁵

¹ Max-Planck-Institut für Radioastronomie, Auf dem Hügel 69, D-53121 Bonn, Germany

² National Radio Astronomy Observatory, Socorro, New Mexico 87801, USA

³ Visiting the Max-Planck-Institut für Radioastronomie, Auf dem Hügel 69, D-53121 Bonn, Germany

⁴ Department of Physics and Astronomy, Hofstra University, Hempstead, NY 11549, USA

⁵ Harvard-Smithsonian Center for Astrophysics, 60 Garden St., MS 42, Cambridge, MA 02138, USA

Received date / Accepted date

Abstract. Using the Effelsberg 100-m telescope, absorption in the $(J,K) = (1,1)$, $(2,2)$ and $(3,3)$ inversion lines of ammonia (NH_3) was detected at a redshift of $z = 0.6847$ toward the gravitational lens system B0218+357. The $\lambda \sim 2$ cm absorption peaks at 0.5–1.0% of the continuum level and appears to cover a smaller fraction of the radio continuum background than lines at millimeter wavelengths. Measured intensities are consistent with a rotation temperature of ~ 35 K, corresponding to a kinetic temperature of ~ 55 K. The column density toward the core of image A then becomes $N(\text{NH}_3) \sim 1 \times 10^{14} \text{ cm}^{-2}$ and fractional abundance and gas density are of order $X(\text{NH}_3) \sim 10^{-8}$ and $n(\text{H}_2) \sim 5 \times 10^3 \text{ cm}^{-3}$, respectively. Upper limits are reported for the $(2,1)$ and $(4,4)$ lines of NH_3 and for transitions of the SO, DCN, OCS, SiO, C_3N , H_2CO , SiC_2 , HC_3N , HC_5N , and CH_3OH molecules. These limits and the kinetic temperature indicate that the absorption lines are not arising from a cold dark cloud but from a warm, diffuse, predominantly molecular medium. The physical parameters of the absorbing molecular complex, seen at a projected distance of ~ 2 kpc to the center of the lensing galaxy, are quite peculiar when compared with the properties of clouds in the Galaxy or in nearby extragalactic systems.

Key words. Galaxies: abundances – Galaxies: ISM – Quasars: individual: B0218+357 – Quasars: absorption lines – Radio lines: galaxies

1. Introduction

With an image separation of 334 mas B0218+357 is one of the most compact gravitational lens systems known to date (O’Dea et al. 1992; Patnaik et al. 1993). The lensed source, possibly a BL Lac object (Kemball et al. 2001), is located at a redshift of $z \sim 0.94$ (Cohen et al. 2003) and shows a complex radio structure with two dominating compact sources, A and B, and an Einstein ring (e.g. Biggs et al. 2001a). A time delay of order 10 days has been measured between the two compact sources (Corbett et al. 1996; Biggs et al. 1999, 2001b; Cohen et al. 2000). Absorption from the lensing galaxy, a face-on spiral likely of type Sa/Sab (York et al. 2005), is observed at a redshift of $z=0.68466$ at optical wavelengths (Brown et al. 1993; Stickel & Kühr 1993) and, remarkably, in the $\lambda 21$ cm line of HI (Carilli et al. 1993) and in numerous radio- and

millimeter-wavelength lines from a variety of molecules. The absorption is observed against the compact component A which is, at radio waves, ~ 3 times stronger than component B (e.g. Patnaik et al. 1993). Detected molecular species are CO, HCN, and HCO^+ (Wiklind & Combes 1995), H_2CO (Menten & Reid 1996), H_2O (Combes & Wiklind 1997), CS (Combes et al. 1997), OH (Kanekar et al. 2003) and tentatively also LiH (Combes & Wiklind 1998). The molecular spectra, combined with 21 cm HI absorption profiles, have been used to constrain the temporal evolution of the fine structure constant (e.g. Carilli et al. 2000; Murphy et al. 2001; Kanekar & Chengalur 2004). The nature of the cloud, however, is poorly understood.

One of the less well known parameters of extragalactic molecular clouds is the kinetic gas temperature. With area filling factors that are not well known, a thermalized tracer like CO cannot be used to determine T_{kin} . Better thermometers are symmetric top molecules, where relative level populations are determined predominantly by collisions. The two most prominent such molecules are NH_3 and CH_3CN . While extragalactic CH_3CN was so far

Send offprint requests to: C. Henkel, e-mail: chenkel@mpifr-bonn.mpg.de

^{*} Based on observations with the 100-m telescope of the Max-Planck-Institut für Radioastronomie (MPIFR) at Effelsberg

Table 1. Observational parameters

ν (GHz)	$\theta_b^a)$ (arcsec)	$T_{\text{sys}}^b)$ (K)	$\eta_a^c)$
5.9	130	35	0.53
13.7–17.8	65–50	50	0.40
21.6–25.8	40–35	50	0.35
43.0–43.2	22	125	0.16

a) Full width to half power (FWHP) beam widths

b) System temperatures in units of antenna temperature (T_A^*)

c) Aperture efficiencies, see the Effelsberg calibration pages in

www.mpifr-bonn.mpg.de

only detected in NGC 253 (Mauersberger et al. 1991), various NH_3 ‘inversion’ lines, from the $(J,K) = (1,1)$ up to the $(6,6)$ and even the $(9,9)$ line, have now been observed in the nuclear regions of nearby ($z \lesssim 0.001$) galaxies (e.g. Martin & Ho 1986; Henkel et al. 2000; Takano et al. 2000, 2002; Weiß et al. 2001; Mauersberger et al. 2003).

B0218+357 provides a unique view onto a molecular cloud seen at about half a Hubble time in the past (Λ -cosmology with $H_0 = 71 \text{ km s}^{-1} \text{ Mpc}^{-1}$, $\Omega_m = 0.27$ and $\Omega_\Lambda = 0.73$; Spergel et al. 2003). In an attempt to constrain the physical properties of this cloud at a luminosity distance of $\sim 3 \text{ Gpc}$, we have searched for NH_3 and other molecular species.

2. Observations

All observations were made with the 100-m telescope at Effelsberg/Germany. In August 2001 and June 2002 we searched, employing a single channel $\lambda \sim 1.9 \text{ cm}$ HEMT receiver, for ammonia (NH_3), sulfur monoxide (SO), methanol (CH_3OH), the SiC_2 radical, cyanodiacetylene (HC_5N) and carbonylsulfide (OCS). The measurements were carried out in a position switching mode. In December 2001 we used a dual channel 1.3 cm HEMT receiver to search for cyanoacetylene (HC_3N) and silicon monoxide (SiO) in its ground vibrational state (see Tables 1 and 2). These measurements were made in a dual beam switching mode with a beam throw of $2'$ and a switching frequency of $\sim 1 \text{ Hz}$. In January 2002, we also employed a single-channel 7 mm HEMT receiver to search for formaldehyde (H_2CO) and deuterated hydrogen cyanide (DCN). These observations were made in a position switching mode. Most recently, in June 2003, a two channel 5 cm HEMT receiver was used to search for the $N=1-0$ $J=3/2-1/2$ transition of the C_3N radical.

Frequencies, beamwidths, system temperatures and aperture efficiencies are given in Table 1. For all measurements we employed an ‘AK 90’ autocorrelator with eight spectrometers, using bandwidths of 40 MHz and 512 channels (20 MHz and 1024 channels and 80 MHz and 256 channels at 5 cm and 7 mm , respectively). Calibration was obtained from measurements of NGC 7027 (Ott et al. 1994).

Pointing corrections could be obtained toward B0218+357 itself and were accurate to better than $10''$.

3. Results

Fig. 1 shows the measured NH_3 profiles. The detected inversion lines, with the ordinate displaying absorption in units of 1% of the continuum flux, are characterized by a prominent narrow component with a width of a few km s^{-1} , centered at slightly positive velocities, and a wider and weaker component that is centered at slightly negative velocities with respect to a redshift of $z=0.68466$. Tables 2 and 3 display noise levels for all measured spectra and line parameters for the detected transitions. The weak but wide velocity component has a 2–3 times higher integrated intensity than the more prominent narrow one. At its peak, the narrow component reaches 0.5–1.0% of the total continuum flux density, while the broad component peaks at $\sim 0.3\%$ in the $(1,1)$ and $(2,2)$ lines and at an even lower level in the $(3,3)$ transition. The narrow component must be optically thin; otherwise the hyperfine satellites would be visible (for the $(1,1)$ line at ± 8 and $\pm 19 \text{ km s}^{-1}$ with respect to the main feature). Due to a lower signal-to-noise ratio, the optical depth of the wide component is poorly constrained (see also Sect. 4.1).

At $\lambda=1.9$ and 1.3 cm , continuum flux densities were 1.0 – 1.2 Jy , in good agreement with Patnaik et al. 1993 and Menten & Reid (1996). At 6 GHz we find 1.45 Jy with an error of $\pm 10\%$, while no flux density was determined at 7 mm .

Fig. 2 shows a Boltzmann plot (rotation diagram) including the four measured ‘metastable’ ($J=K$) inversion lines of ammonia. Applying

$$N(J,K)/T_{\text{ex}} = 1.61 \times 10^{14} \frac{J(J+1)}{K^2 \nu} \int \tau dV$$

($N(J,K)$ in cm^{-2} , T_{ex} in K, ν in GHz; see e.g. Hüttemeister et al. 1995) and assuming optically thin absorption (see Sect. 4.1) and equal excitation temperatures (T_{ex}) across the measured inversion doublets, rotation temperatures are of order 35 – 40 K . Although the $(1,1)$ and $(2,2)$ lines belong to the para- and the $(3,3)$ line to the ortho-species (the conversion from one to the other species takes very long; see Cheung et al. 1969), no difference in excitation is apparent. The upper limits to the $(4,4)$ line are consistent with the rotation temperature derived from the lower inversion transitions.

4. Molecular cloud properties

4.1. Location and linewidth

Prior to this study, Menten & Reid (1996) had searched for NH_3 absorption towards B0218+357. Their upper limits are higher than the strength of the absorption features shown in Fig. 1. It is tempting to identify the two main features of the NH_3 lines as absorption against the two dominant continuum sources A and B. However, this is

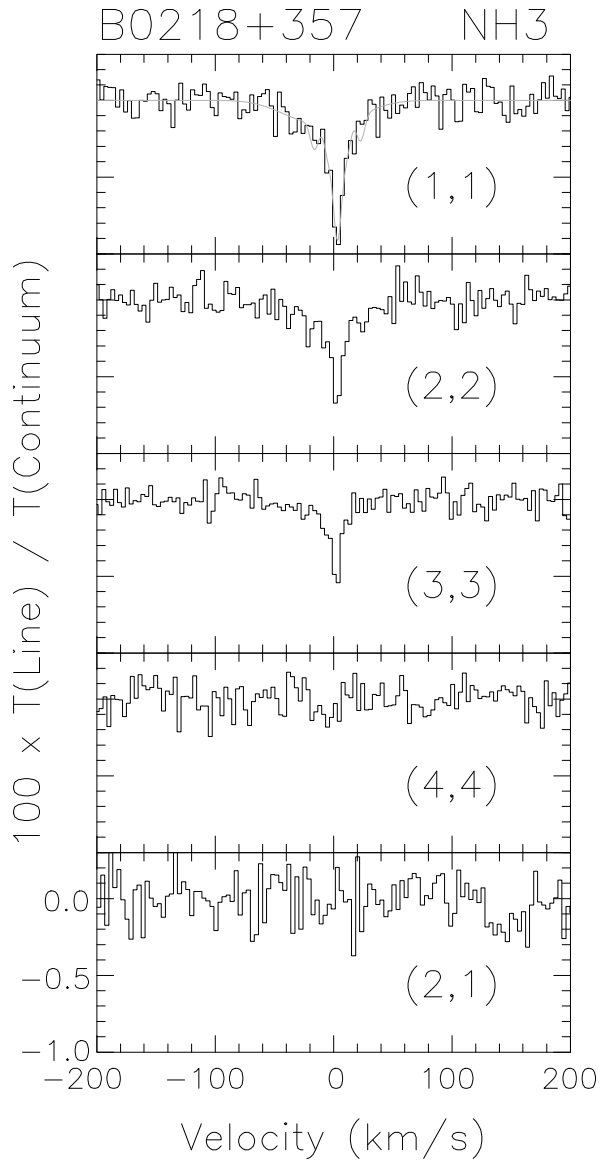


Fig. 1. NH_3 lines with a velocity scale relative to $z=0.68466$, observed towards B0218+357. Channel widths are 3.3 km s^{-1} . The ordinate is in units of the radio continuum flux. In the case of the (1,1) line a two component fit has been added accounting for NH_3 hyperfine splitting (Kukolich 1967). The fit demonstrates that the line profile is consistent with two optically thin velocity features. Limited signal-to-noise ratios do not constrain the fit sufficiently to justify an inclusion of its parameters in Table 3.

extremely unlikely for several reasons. VLBI observations of HI at dm- and of H_2CO at cm-wavelengths have shown that the absorption is confined to image A (Carilli et al. 2000; Menten & Reid 1996). While at radio wavelengths image A is three times as bright as B, image B is brighter at optical wavelengths. This indicates that image A is obscured by dust. Heavy absorption of A is further supported by a large differential rotation measure between A and B (Patnaik et al. 1993) and by the different separations be-

Table 2. rms line to continuum ratios in units of $10^3 \times [\text{rms}/T_c]$ (Col. 4) and corresponding channel spacings (Col. 5)

Molecule	Line	ν (GHz)	rms (10^{-3})	Channel width (km s^{-1})
C_3N	$N=1-0, J=3/2-1/2$	5.868	3.0	2.29
NH_3	$(J, K)=(2, 1)$	13.711	2.1	1.71
CH_3OH	$J_{K_a K_c}=9_2-10_1 \text{ A}^+$	13.724	1.8	1.71
SiC_2	$J_{K_a K_c}=1_{01}-0_{00}$	14.009	2.0	1.65
NH_3	$(J, K)=(1, 1)$	14.065	1.0	1.65
NH_3	$(J, K)=(2, 2)$	14.082	1.1	1.65
NH_3	$(J, K)=(3, 3)$	14.169	0.7	3.30
HC_5N	$J=9-8$	14.225	1.3	3.30
NH_3	$(J, K)=(4, 4)$	14.329	1.4	1.65
OCS	$J=2-1$	14.440	1.9	1.65
SO	$J_K=1_0-0_1$	17.809	2.6	1.32
HC_3N	$J=4-3$	21.602	8.2	1.08
SiO	$J=1-0, v=0$	25.776	20.2	0.91
DCN	$J=1-0$	42.985	16.7	2.18
H_2CO	$J_{K_a K_c}=1_{01}-0_{00}$	43.236	222.7	2.17

Table 3. NH_3 line parameters^{a)}

Line	$\int \tau dV$	V (km s^{-1})	$\Delta V_{1/2}$
NH_3 (1,1)	-0.062 (0.013)	+3.3 (0.5)	9.3 (1.8)
	-0.183 (0.019)	-2.0 (2.7)	56.6 (7.8)
NH_3 (2,2)	-0.037 (0.009)	+3.1 (0.5)	6.6 (1.6)
	-0.143 (0.017)	-1.7 (3.0)	54.7 (7.6)
NH_3 (3,3)	-0.034 (0.011)	+2.4 (0.5)	7.3 (2.3)
	-0.070 (0.013)	-5.8 (5.8)	46.2 (14.1)

a) From Gaussian fits adopting $z=0.68466$ and assuming that the continuum source covering factor is $f_c=1$. Standard deviations are given in parenthesis.

tween images A and B at radio and optical wavelengths (334 ± 1 versus $317 \pm 2 \text{ mas}$, respectively; York et al. 2005). Apparently, radio and optical images of A do not coincide. We further note that images A and B are on opposite sides of the lensing galaxy. Assuming a rotation velocity of order $\gtrsim 150 \text{ km s}^{-1}$, a difference in radial velocity of $\sim 5 \text{ km s}^{-1}$ between images A and B would then require an inclination $i \lesssim 1^\circ$ for the lensing galaxy. While the galaxy is clearly face-on (York et al. 2005), the optical image does not require an inclination that close to zero.

We conclude that the two velocity components are associated with image A that shows a core-jet morphology (Patnaik et al. 1995; Porcas & Patnaik 1995; Biggs et al. 2003). While the stronger narrower velocity component has a linewidth that is well within the range observed in galactic giant molecular clouds (e.g. Combes 1991), the linewidth of the broad component is much larger. Could this be a consequence of hyperfine splitting of the ammonia lines? Or a consequence of differential galactic rotation?

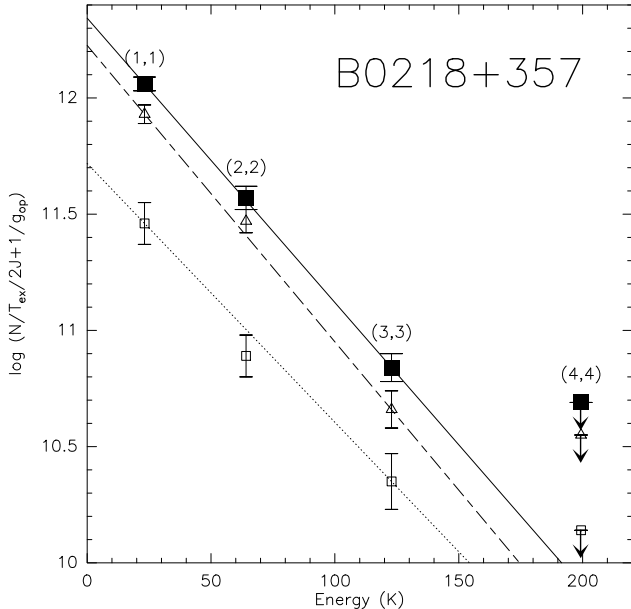


Fig. 2. Boltzmann plot (rotation diagram) of the normalized NH_3 column density (g_{op} is 1 for para- NH_3 ($K = 1, 2, 4$) and 2 for ortho- NH_3 ($K = 3$)) divided by the excitation temperature T_{ex} in K within the inversion doublet as a function of excitation above the ground state. Lines connect the $(J, K) = (1, 1)$ and $(3, 3)$ normalized column densities (the $(4, 4)$ transition was not detected). Filled squares connected by a solid line: total NH_3 absorption; open triangles connected by a dashed line: broad NH_3 absorption component; open squares connected by a dotted line: narrow NH_3 absorption component. Assuming optically thin absorption and equal excitation temperatures in the inversion doublets, rotation temperatures become $35.5 \pm 2.5 \text{ K}$ (total), $34.0 \pm 2.9 \text{ K}$ (broad component) and $39.0 \pm 6.2 \text{ K}$ (narrow component).

The NH_3 hyperfine satellites (for a $(J, K) = (1, 1)$ spectrum, see e.g. Ho & Townes 1983) are symmetrically bracketing the main feature and are covering $\sim 40 \text{ km s}^{-1}$. Thus the partially blended satellite features from *both* velocity components can explain the observed linewidths of $\sim 50 \text{ km s}^{-1}$. For a clear separation of individual satellite lines and velocity components, data with higher signal-to-noise ratios would be required.

The jet extends from the core of A over $\sim 6 \text{ mas}$ toward the center of the lensing foreground galaxy, located at an angular distance of almost 300 mas (Patnaik et al. 1995; Porcas & Patnaik 1995; Biggs et al. 2003; Wucknitz et al. 2004). Position angles are $\sim 68^\circ$ for the jet (Biggs et al. 2003) and $65^\circ \pm 2^\circ$ for the center (Wucknitz et al. 2004). Therefore no significant velocity gradient is expected from the foreground galaxy. Its low inclination further reduces any such gradient. A wide component with an FWHM linewidth of order 50 km s^{-1} is not seen in other molecular lines at cm- and mm-wavelengths (e.g. Wiklind & Combes 1995; Menten & Reid 1996). Thus hyperfine splitting is likely the main cause for the linewidths observed. Note,

that there are indications for the same asymmetry, i.e. a stronger feature at slightly positive and a weaker feature at slightly negative velocities, in the CO $J=2-1$ and $3-2$, HCN $2-1$ and HCO^+ $2-1$ lines (Wiklind & Combes 1995; Combes & Wiklind 1997, 1998).

To summarize: While the relatively strong narrow absorption component at slightly positive velocities (see Fig. 1) must be optically thin, the optical depth of the wider and weaker component remains undetermined. Total linewidths are greatly affected by the spacing of the hyperfine features. Gaussian fits to the wide component (Table 3) include the hyperfine satellites of both velocity components.

4.2. Cloud size, optical depth and source covering factor

Molecular lines at mm-wavelengths can show deep absorption (Combes & Wiklind 1995; Wiklind & Combes 1995; Combes & Wiklind 1997). Lines at dm- and cm-wavelengths are generally weaker with respect to the continuum. This even holds for $\lambda=21 \text{ cm}$ HI and 18 cm OH, that show wider absorption than ammonia and the mm-wave lines (Carilli et al. 1993; Kanekar et al. 2003) and that may thus arise from a larger volume. The peak line to total continuum ratios of the 18 cm OH main lines are, however, similar to those seen in ammonia.

Since the continuum sources are compact and since the measured NH_3 linewidths are small by extragalactic standards, the absorption arises from an area that must be considerably smaller than that studied in emission with single-dish telescopes towards nearby galaxies. According to Patnaik et al. (1995), $\sim 70\%$ of the total 22 GHz flux is associated with image A. Thus minimum optical depths and source covering factors ($f_{\text{c,cm}}$) of the ammonia lines toward image A are a factor of 1.4 higher than those suggested for the entire continuum flux by Fig. 1. They reach, in the $(1, 1)$ line, $\gtrsim 0.014$.

Sensitive maps of image A show a source of size $10 \times 10 \text{ mas}^2$ that is edge-brightened on its south-western side and tangentially stretched (Biggs et al. 2003). At 15 GHz , the south-eastern region containing the core (components A1 and A2) and the north-western region containing the jet exhibit $62 \pm 1\%$ and $38 \pm 5\%$ of the observed flux density, respectively (Patnaik et al. 1995). Although higher frequency VLBI measurements are missing, it would be no surprise if the contribution of the jet in image A is negligible at $100\text{--}150 \text{ GHz}$, thus leaving only the lensed core as the background continuum source. Assuming for the core component a brightness temperature T_{b} and a flux density S_{ν} not drastically varying with frequency in the $10\text{--}150 \text{ GHz}$ frequency range (see e.g. Blandford & Königl 1979), its solid angle would vary like $\Omega \propto \nu^{-2 \dots -1}$ (see also Lobanov 1998). According to

NED¹ the mm-wave flux of B0218+357 is about half of that at cm-wavelengths, compatible with a fading jet and a flat spectrum core.

Adopting this scenario and assuming that the absorption arises exclusively from the core as it is indicated by some of the deep mm-wave absorption lines (CO should arise from a larger volume than NH₃), we obtain for the peak of the ammonia (1,1) line a minimum optical depth and covering factor of $0.01/(0.7 \times 0.62) = 0.023$. At 150 GHz, this would yield for a cloud centered near the peaks of image A $f_{c,mm} \gtrsim 0.15$ –1.0, depending on whether the exponent in the frequency dependence of the solid angle Ω is -1 or -2 .

High source covering factors at mm-wavelengths can be achieved, if the molecular absorber is elongated along the same position angle as the continuum, i.e. along a path with roughly constant galactocentric radius, hypothetically defining a spiral arm (see also Sect. 5). Elongated filaments are common in the Galaxy and are exemplified by the morphology of the Orion giant molecular cloud or the connection between this GMC and the Monoceros GMC (Maddalena & Thaddeus 1985), reaching linear sizes in excess of 100 pc. This is more than the few 10 pc that are needed here. Observed $f_{c,mm}$ values near unity then suggest that actual source covering factors ($f_{c,mm}$ and $f_{c,cm}$) are 1–6 times higher than the lower limits estimated above, not providing an additional constraint for the NH₃ source covering factor.

To verify these estimates and to further elucidate the morphology of image A and its foreground molecular cloud at high frequencies, mm-wave VLBI observations are highly desirable.

4.3. Densities and column densities

So far, the nature of the molecular cloud has been an enigma. It was proposed to be either a diffuse or a dark cloud (Combes & Wiklind 1995; Wiklind & Combes 1995; Menten & Reid 1996; Kanekar et al. 2003). The determination of an NH₃ rotation temperature, which is a lower limit to the kinetic temperature, allows us to discriminate between these two scenarios. Provided total gas densities are less than $n(\text{H}_2) \sim 10^6 \text{ cm}^{-3}$ and using the Large Velocity Gradient (LVG) model of Schilke (1989) with collision rates from Danby et al. (1988), the kinetic temperature is 50–60 K. For even higher densities the kinetic temperature would be lower but would still be >35 K. Since frequencies of the ammonia lines are quite similar, the resulting temperatures are not significantly affected by potential differences in the morphology of the background continuum. We therefore conclude that the NH₃ absorption *does not arise from a cool dark cloud*. Since the HCO⁺ absorption lines are not fully saturated (Wiklind & Combes 1995) and many molecules have not been detected at levels of

$<1\%$ of the total continuum flux density (Table 2), *the diffuse cloud scenario is preferable*.

The high kinetic temperature of the gas implies that our non-detection of the DCN $J=1-0$ line does not provide significant constraints to the cosmic D/H ratio. Adopting a width of the line of order 5 km s^{-1} , we deduce a 5σ sensitivity of 5% of the continuum level (Table 2). Assuming an optical depth of 5 for the opacity of the HCN $J=1-0$ main line, this implies that we would have seen a DCN line only if $[\text{DCN}]/[\text{HCN}] \gtrsim 10^{-2}$. A ratio of 10^{-2} is, however, not reached at $T_{\text{kin}}=20$ K (Gerin et al. 1999) and $[\text{DCN}]/[\text{HCN}]$ ratios at higher temperatures should be even smaller.

Having estimated the kinetic temperature, we can use measurements of molecular excitation to also obtain the density of the gas toward B0218+357. From the microwave background we obtain a minimum of $T_{\text{cmb}} = 2.73(1+z) = 4.6$ K. Combes et al. (1997) find $T_{\text{ex}} = 6_{-2}^{+3}$ K from CS $J=1-0$ and $3-2$. The detection of the 557 GHz and the non-detection of the 183 GHz line of water vapor (these are rest frequencies) indicate $T_{\text{ex}} < 30$ K (Combes & Wiklind 1997). ¹³CO $J=2-1$ and $4-3$ spectra suggest $T_{\text{ex}} < 20$ K (Gerin et al. 1997). With $T_{\text{kin}} \gtrsim 35$ K and $n(\text{H}_2) \gtrsim 10^6 \text{ cm}^{-3}$, LVG calculations for CS (for details, see e.g. Wang et al. 2004) yield an excitation far above that observed. Thus $T_{\text{kin}} \sim 55$ K. With this kinetic temperature and $T_{\text{ex,CS}} \leq 9$ K, $n(\text{H}_2) \lesssim 2 \times 10^4 \text{ cm}^{-3}$. This is a firm upper limit. If the excitation is close to 6 K or if the stronger CS line ($J=1-0$) is optically thick, densities are smaller ($\sim 7 \times 10^3 \text{ cm}^{-3}$ in the former case), while constraints from H₂O are less stringent. Again using LVG calculations, we find that a density of $\sim 5 \times 10^3 \text{ cm}^{-2}$ is consistent with ¹³CO excitation temperatures $\lesssim 20$ K, if optical depths are smaller than unity. Since Combes & Wiklind (1995) find that the ¹³CO $J=2-1$ line is saturated, however, the density will be even lower. The upper density limits derived here are also consistent with the upper limit to the NH₃ (2,1) line (Fig. 1 and Table 2), that would only be detectable in a cloud with much higher density (see Mauersberger et al. 1985).

Adopting $T_{\text{kin}}=55$ K and, less certain, $n(\text{H}_2)=5 \times 10^3 \text{ cm}^{-3}$ as best guesses, we can also estimate the excitation temperature within an NH₃ inversion doublet: $T_{\text{ex}} \sim 6$ K (Schilke 1989, his Fig. 6.15). This can be used to derive total NH₃ column densities. Adding up column densities in the three detected lines gives $N(\text{NH}_3) = 4 \times 10^{13} \text{ cm}^{-2}$. This is a minimum value. With equation A15 of Ungerechts et al. (1986) and rotation temperatures of $T_{12}=35$ –40 K, we obtain $\sim 5 \times 10^{13} \text{ cm}^{-2}$. The error lies mainly in the assumed density of the gas. $n(\text{H}_2)=10^4 \text{ cm}^{-3}$ implies an excitation temperature of 8 K and a column density of 5 and $7 \times 10^{13} \text{ cm}^{-2}$, respectively. So far all given column densities are averaged over the entire continuum source. Averaged over the core of image A, column densities have to be multiplied by a factor of 2.3.

Typical galactic clouds have fractional abundances of $X(\text{NH}_3) = 10^{-8}$ – 10^{-7} (e.g. Hotzel et al. 2004). Averaged

¹ This research made use of the NASA/IPAC Extragalactic Database (NED) which is operated by the Jet Propulsion Laboratory, CalTech, under contract with NASA.

over the entire continuum source, this yields $N(\text{H}_2) \sim 4 \times 10^{20} - 7 \times 10^{21} \text{ cm}^{-2}$ or $1 \times 10^{21} - 2 \times 10^{22} \text{ cm}^{-2}$ for the core of image A. The lower limit is too small to allow us to detect a variety of molecular lines. Therefore the fractional abundance is likely close to 10^{-8} . Our column density range is slightly lower than what has been proposed by Menten & Reid (1996) on the basis of another molecular cm-wave transition. Adopting 55 K also for the HI spin temperature, the total background continuum averaged HI column density becomes $2 \times 10^{20} \text{ cm}^{-2}$ (see Carilli et al. 1993). Accounting for an image A core source covering factor, the column density becomes $5 \times 10^{20} \text{ cm}^{-2}$. Thus the line of sight must be mostly molecular.

Column densities averaged over the extent of the continuum source are lower at cm-wavelengths (see Menten & Reid 1996) than those derived by the higher frequency studies of Gerin et al. (1997), $\gtrsim 2 \times 10^{22} \text{ cm}^{-2}$, and Combes & Wiklind (1995), $\sim 5 \times 10^{23} \text{ cm}^{-2}$. This is expected for a molecular cloud located near the peak of image A and covering most of the mm-wave but only a fraction of the cm-wave continuum of B0218+357. In spite of this effect the value proposed by Combes & Wiklind (1995), $N(\text{H}_2) \sim 5 \times 10^{23} \text{ cm}^{-2}$, must be too large. With such an enormous column density many of the species listed in Table 2 would have been detected. The $^{18}\text{O}/^{17}\text{O}$ ratio of ~ 15 suggested by Combes & Wiklind (1995), that is in part responsible for the high column density, is far outside the range observed so far in interstellar clouds. With $^{18}\text{O}/^{17}\text{O} \sim 1.6$ in the LMC (Heikkilä et al. 1998), ~ 4.1 in the local interstellar medium (Wouterloot et al. 2005), 5.5 in the solar system (e.g. Wilson & Rood 1994), and ~ 6.5 in nearby starburst galaxies (Harrison et al. 1999; Wang et al. 2004), new measurements of rare CO isotopomers would thus be desirable.

5. A comparison with ‘local’ molecular clouds

To put our data into context with the much more extensively studied interstellar medium of the local universe is not easy. The kinetic temperature we derive, ~ 55 K, is much higher than the canonical number of 10 K assumed for quiescent Giant Molecular Cloud gas in the Galaxy. Clouds forming massive stars are warmer and may reach 55 K, but densities tend to be larger than those estimated in Sect. 4.3 for B0218+357.

The central region of the irregular starburst galaxy M 82 may provide the best agreement with the molecular parameters of B0218+357. In M 82, NH_3 observations indicate $T_{\text{rot}} \sim 30$ K and $T_{\text{kin}} \sim 50$ K (Weiß et al. 2001), while observations of CO reveal densities of several 10^3 cm^{-3} (e.g. Mao et al. 2000). The interstellar medium of M 82 is characterized by widespread PDRs (photon dominated regions/photodissociation regions), where ammonia, being readily destroyed by UV photons, mostly resides in the few remaining well shielded relatively cool cloud cores. Fractional ammonia abundances are of order 5×10^{-10} and thus much lower than in B0218+357. In the inner few 100 pc of nearby spiral galaxies, detected in NH_3 ,

temperatures are significantly higher than in B0218+357 ($T_{\text{rot}} > 35$ K; $T_{\text{kin}} > 55$ K; Mauersberger et al. 2003). This also holds for clouds within a few 100 pc of the center of our Galaxy (Güsten et al. 1985; Mauersberger et al. 1986; Hüttemeister et al. 1993).

In the Galaxy, few measurements of NH_3 absorption from diffuse clouds against radio continuum sources have been reported and neither this molecule’s abundance (if detected) nor its rotation temperature are known in such environments (Nash 1990). It would thus be easiest to reconcile our NH_3 results with a known scenario if we assumed that the B0218+357 absorption line of sight crossed the central region of the lensing galaxy. This, however, is not the case. Wucknitz et al. (2004) model the B0218+357 system using the LENCLEAN algorithm and find the lens to be centered at a position which is $(\Delta\alpha, \Delta\delta) = (255, 120)$ mas offset from the A image and $(-55, -10)$ mas from the B image, with uncertainties of order 5 mas in each coordinate. The best fit size of the lens is 258×121 mas with a position angle of $\text{PA} = -48^\circ$ east of north (Wucknitz et al. 2004, Table 4). This implies that image A is at a projected distance of ~ 2.0 kpc ($\text{P.A.} = -115^\circ$) from the center of the lensing mass distribution, while image B is offset by only 0.4 kpc ($\text{PA} = +70^\circ$). Since the starburst in M 82 is, as most starbursts, confined to the nuclear few 100 pc and since its fractional NH_3 abundance is much smaller than that in B0218+357, we do not find, neither in the Galaxy nor in the nearby extragalactic universe, any analog to the line-of-sight toward image A in B0218+357.

6. Conclusions

The gravitational lens system B0218+357 allows us to study the details of a molecular cloud observed at about half a Hubble time in the past. Our analysis of the Effelsberg data reveals the following:

- Ammonia (NH_3) is detected in absorption in its three lowest metastable inversion doublets, while the $(J, K) = (4, 4)$ and the non-metastable $(2, 1)$ lines remain undetected. Upper limits are also determined for transitions of SO, DCN, OCS, SiO, C_3N , H_2CO , SiC_2 , HC_3N , HC_5N , and CH_3OH .
- NH_3 is likely absorbing exclusively the core of image A. Source covering factors and peak optical depths are $\gtrsim 0.023$ toward this core.
- The NH_3 rotation temperature of $T_{\text{rot}} \sim 35$ K indicates a kinetic temperature of $T_{\text{kin}} \sim 55$ K for the molecular gas.
- With the kinetic temperature obtained from NH_3 , the measured excitation of other molecular species can be used to constrain the density. $n(\text{H}_2) \sim 5 \times 10^3$ is found to be a plausible value. Averaged over the entire continuum source, the NH_3 column density is $N(\text{NH}_3) \sim 5 \times 10^{13} \text{ cm}^{-2}$; averaged over the core of image A, it is $\sim 1 \times 10^{14} \text{ cm}^{-2}$ with a fractional abundance of order 10^{-8} . The gas along the line of sight is predominantly molecular.

- The physical parameters are quite peculiar, when compared with those of clouds in the local universe.
- Because the morphology of the radio continuum depends on frequency, cm-wave and mm-wave absorption features are characterized by different H₂ column densities.

Acknowledgements. We wish to thank R. Porcas, C. Böttner, M. Kadler and T. Krichbaum for useful discussions and an anonymous referee for critically reading the text and making a number of important suggestions.

References

- Biggs, A. D., Browne, I. W. A., Helbig, P., et al. 1999, *MNRAS*, 304, 349
- Biggs, A. D., Browne, I. W. A., Muxlow, T. W. B., & Wilkinson, P. N. 2001a, *MNRAS*, 322, 821
- Biggs, A. D., Browne, I. W. A., & Wilkinson, P. N. 2001b, *MNRAS*, 323, 995
- Biggs, A. D., Wucknitz, O., Porcas, R. W. et al. 2003, *MNRAS*, 338, 599
- Blandford, R. D., Königl, A. 1979, *ApJ*, 232, 34
- Browne, I. W. A., Patnaik, A. R., Walsh, D., & Wilkinson, P.N. 1993, *MNRAS*, 263, L32
- Carilli, C. L., Rupen, M. P., & Yanni, B. 1993, *ApJ*, 412, L59
- Carilli, C. L., Menten, K. M., Stocke, J. T., et al. 2000, *Phys. Rev. Lett.*, 85, 5511
- Cheung, A. C., Rank, D. M., Townes, C. H., Knowles, S. H., & Sullivan, W. T. 1969, *ApJ*, 157, L13
- Cohen, A. S., Hewitt, J. N., Moore, C. B., & Haarsma, D. B. 2000, *ApJ*, 545, 578
- Cohen, J. G., Lawrence, C. R., & Blandford, R. D. 2003, *ApJ* 583, 67
- Combes, F. 1991, *ARA&A*, 29, 195
- Combes, F., & Wiklind, T. 1995, *A&A*, 303, L61
- Combes, F., & Wiklind, T. 1997, *ApJ*, 486, L79
- Combes, F., Wiklind, T., & Nakai, N. 1997, *A&A* 327, L17
- Combes, F., & Wiklind, T. 1998, *A&A*, 334, L81
- Corbett, E. A., Browne, I. W. A., Wilkinson, P. N., & Patnaik, A. R. 1996, in *Astrophysical Applications of Gravitational Lensing*, IAU Symp. 173, eds. C.S. Kochanek & J.N. Hewitt, Kluwer Academic Publishers, Dordrecht, p37
- Danby, G., Flower, D. R., Valiron, P., Schilke, P., Walmsley, C.M. 1988, *MNRAS*, 235, 229
- Gerin, M., Phillips, T. G., Benford, D. J., et al. 1997, *ApJ*, 488, L31
- Gerin, M., & Roueff, E. 1999, in *Highly Redshifted Radio Lines*, ASP Conf. Ser. 156, eds. C. Carilli et al., San Francisco, p196
- Güsten, R., Walmsley, C. M., Ungerechts, H., & Churchwell, E. 1985, *A&A*, 142, 381
- Harrison, A., Henkel, C., & Russel, A. 1999, *MNRAS*, 303, 157
- Heikkilä, A., Johansson, L.E.B., & Olofsson, H. 1998, *A&A*, 332, 493
- Henkel, C., Mauersberger, R., Peck, A. B., Falcke, H., & Hagiwara, Y. 2000, *A&A*, 361, L45
- Ho, P. T. P., & Townes, C. H. 1983, *ARA&A*, 21, 239
- Hotzel, S., Harju, J., & Walmsley, C. M. 2004, *A&A*, 415, 1065
- Hüttmeister, S., Wilson, T. L., Henkel, C., Mauersberger, R. 1993, *A&A*, 276, 445
- Hüttmeister, S., Wilson, T. L., Mauersberger, R., et al. 1995, *A&A*, 294, 667
- Kanekar, N., Chengalur, J. N., de Bruyn, A. G., & Narasimha, D. 2003, *MNRAS*, 345, L7
- Kanekar, N., & Chengalur, J. N. 2004, *MNRAS*, 350, L17
- Kemball, A. J., Patnaik, A. R., & Porcas, R. W. 2001, *ApJ*, 562, 649
- Kukulich, S. G. 1967, *Phys. Rev.*, 156, 83
- Lobanov, A. P. 1998, *A&A*, 330, 79
- Maddalena, R. J., & Thaddeus, P. 1985, *ApJ*, 294, 231
- Martin, R. N., & Ho, P. T. P. 1986, *ApJ*, 308, L7
- Mao, R. Q., Henkel, C., Schulz, A., et al. 2000, *A&A*, 358, 433
- Mauersberger, R., Wilson, T. L., Walmsley, C. M., Henkel, C. & Batrla, W. 1985, *A&A*, 146, 168
- Mauersberger, R., Henkel, C., Wilson, T. L., Walmsley, C. M. 1986, *A&A*, 162, 199
- Mauersberger, R., Henkel, C., Walmsley, C. M., Sage, L.J., & Wiklind, T. 1991, *A&A*, 247, 307
- Mauersberger, R., Henkel, C., Weiß, A., Peck, A. B., & Hagiwara, Y. 2003, *A&A*, 403, 561
- Menten, K. M., & Reid, M. J. 1996, *ApJ*, 465, L99
- Murphy, M. T., Webb, J. K., Flambaum, V. V. et al. 2001, *MNRAS* 327, 1244
- Nash, A. G. 1990, *ApJS* 72, 303
- O’Dea, C. P., Baum, S. A., Stanghellini, C., et al. 1992, *AJ*, 104, 1320
- Ott, M., Witzel, A., Quirrenbach, A., et al. 1994, *A&A*, 284, 331
- Patnaik, A. R., Browne, I. W. A., King, L. J., et al. 1993, *MNRAS*, 261, 435
- Patnaik, A. R., Porcas, R. W., & Browne, I. W. A. 1995, *MNRAS*, 274, L5
- Porcas, R. W., & Patnaik, A. R. 1995, in *Astrophysical Applications of Gravitational Lensing*, IAU Symp. 173, eds. C.S. Kochanek & J.N. Hewitt, Kluwer Academic Publishers, Dordrecht, p311
- Schilke, P. 1989, Diploma Thesis, Univ. of Bonn
- Spergel, D. N., Verde, L., Peiris, H. et al. 2003, *ApJS* 148, 175
- Stickel, M., & Kühr, H. 1993, *A&AS*, 101, 521
- Takano, S., Nakai, N., Kawaguchi, K., & Takano, T. 2000, *PASJ*, 52, L67
- Takano, S., Nakai, N., & Kawaguchi, K. 2002, *PASJ*, 54, 195
- Ungerechts, H., Winnewisser, G., & Walmsley, C.M. 1986, *A&A* 157, 207
- Wang, M., Henkel, C., Chin, Y.-N., et al. 2004, *A&A*, 422, 883
- Weiß, A., Neininger, N., Henkel, C., Stutzki, J., & Klein, U. 2001, *ApJ*, 554, L143
- Wiklind, T., & Combes, F. 1995, *A&A*, 299, 382
- Wilson, T. L., & Rood, R. 1994, *ARA&A*, 32, 191
- Wouterloot, J. G. A., Brand, J., & Henkel, C. 2005, *A&A*, 430, 549
- Wucknitz, O., Biggs, A. D., & Browne, I. W. A. 2004, *MNRAS*, 349, 14
- York, T., Jackson, N., Browne, I. W. A., Wucknitz, O., & Skelton, J. E. 2005, *MNRAS*, 357, 124